Fracture of Polymers, Composites and Adhesives II
B.R.K. Blackman, A. Pavan and J.G. Williams (Eds)

3D MODELLING OF IMPACT FAILURE IN SANDWICH STRUCTURES

C. YU*, M. ORTIZ and A.J. ROSAKIS
*E. T. S. de Ingenieros, Canales y Puertos, Universidad de Castilla-La Mancha
13071 Ciudad Real, Spain
Graduate Aeronautical Laboratories, California Institute of Technology
Pasadena, CA 91125, USA

ABSTRACT

Cohesive theories of fracture are applied to simulate the complex failure modes in sandwich structures subjected to low-speed impact. The particular configuration contemplated in this study refers to the experiments performed by Xu and Rosakis [1], where the model specimens involving a compliant polymer core sandwiched between two metal layers, were adopted to simulate failure evolution mechanisms in real sandwich structures. Fracture has been modeled by recourse to an irreversible cohesive law embedded into three-dimensional cohesive elements. These cohesive elements govern all aspects of the separation of the incipient cracks. The cohesive behavior of the material is assumed to be rate independent and, consequently, all rate effects predicted by the calculations are due to inertia. The fidelity of the model has been validated by several previous simulations [2,3]. The numerical simulations have proved highly predictive of a number of observed features, including: the complex sequences of the failure mode, shear-dominated inter-sonic (a speed that is greater than shear wave speed but less than the longitudinal wave speed of the material) inter-layer cracks, the transition from inter-layer crack growth to intra-layer crack formation and the core branching later on.

KEYWORDS

Impact failure, sandwich structures, intra-layer crack, inter-layer crack, finite elements and cohesive elements.

INTRODUCTION

Sandwich structures have relative advantages over other structural materials in terms of improved stability, weight savings, crash worthiness and corrosion resistance. Therefore layered materials and sandwich structures have diverse and technologically interesting applications in many areas of engineering. These includes the increased use of composite laminates in aerospace and automotive engineering; the introduction of layered concrete pavements in civil engineering; the use of thin films and layered structures in micro-electric components, and very recently, the introduction of naval engineering applications like nonferrous ship hulls [1].

However, one of the shortcomings of sandwich structures is the still incomplete understanding of damage, as it can develop as a consequence of low-velocity impacts (such as tool drops) or high-energy events (such as ballistic penetration) or an unusual level of the design loading. The damage characterization of sandwich structures is certainly more complicated than the one of conventional laminates. A first reason, related to their special structure, is that the damage often does not develop uniformly across the thickness. A second reason is that besides typical failure modes (such as penetration and de-lamination), also crushing and facet sheets de-bonding must be addressed. The shear load transfer through the core is often combined with unsymmetrical damage, which requires a detailed study in order to understand the damage progression and evaluate the residual strength.

Motivated by those concerns, Xu and Rosakis [1] conducted a series of experiments investigating the generation and subsequent evolution of dynamic failure modes in layered materials subjected to impact. Model experiments in plane stress configuration were chosen to simplify the 3D problem of the out-of-plane impact of the real sandwich structures. High-speed photography and dynamic photo-elasticity were utilized to study the nature and sequence of the failure modes. A series of complex failure modes were documented. They found that in all cases, the dominant dynamic failure mode is the *inter-layer* failure (de-lamination between panel and core), which is shear-driven and proceeds at inter-sonic speed even under moderate impact speeds. The shear inter-layer cracks kinked into the core layer, propagated as opening-dominated *intra-layer* cracks and eventually branched as they attained high enough growth speeds causing more fragmentation [1]. The effects of impact speed and interfacial bond strength on the dynamic failure of model sandwich structures were also reported.

Cohesive theories have been proved to be one of the most appealing and reliable approaches to the numerical simulation of complex fracture processes. Cohesive models furnish a complete theory of fracture which is not limited by any consideration of material behavior, finite kinematics, non-proportional loading, dynamics, or geometry of the specimen. In addition, cohesive theories fit naturally within the conventional framework of finite-element analysis, and have proved effective in the simulation of complex fracture processes [2,3]. Cohesive theories are characterized by an intrinsic length scale and an intrinsic time scale. The accurate description of fracture processes by means of cohesive elements requires the resolution of the characteristic cohesive length of the material [4,5]. In some materials, such as ceramics and glass, this length may be exceedingly small. Thus calculations based on cohesive elements inevitably have a *multi-scale* character, in as much as the numerical model must resolve two disparate length scales commensurate with the macroscopic dimensions of the solid and the cohesive length of the material. The intrinsic time scale, in conjunction with inertia, introduces a rate dependency able to modify the response of the model for slow and fast processes.

Another interesting feature of the finite-element model adopted is the explicit treatment of fracture and fragmentation [6,7]. It tracks individual cracks as they nucleate, propagate, branch, and possibly link up to form fragments. It is incumbent upon the mesh to provide a rich enough set of possible fracture paths, since the model allows de-cohesion to occur along element boundaries only. However, no mesh dependency is expected as long as the cohesive elements adequately resolve the fracture process zone of the material [5]. It is also interesting to notice that the micro inertia attendant to the material in the dynamic fragmentation process contributes to the correct simulation of the rate effects [2,3].

The simulations in this paper give failure modes sequences very similar to the actual ones observed in the experiments. The model predicts the formation of shear-dominated inter-layer (or interfacial) cracks that initiate first and that such cracks grow very dynamically, their speeds and shear nature being enhanced by the large wave mismatch between the core and the face sheet. The triggering of the complex mechanism of the intra-layer failure of the core structure is also well reproduced.

The organization of the paper is the following. The material characteristics and the dynamic experimental setup are described in the next section. Finite element implementations are presented afterwards and the simulation results and the comparisons with the experiments are discussed at the end.

EXPERIMENTAL SETUP

Material description

The sandwich specimen used in the experiments of Xu and Rosakis [1] is a thin plate obtained by bonding along their thickness two 4340-steel (external) plates to an Homalite-100 (internal) plate. The geometry for a typical specimen used in the experiments is shown in Fig. 1. Both steel and Homalite are characterized by elastic material properties, reported in Table 1 [1]. The fracture parameters for the two bulk materials and the interface bond Weldon-10 adopted in the experiments are reported in Table 2 [1], where σ_c is the maximum cohesive stress or static tensile strength of the material; τ_c is the maximum shear stress; δ_c is critical opening displacement of the cohesive law; K_{Ic} is the fracture toughness; G_c is the fracture energy; R is the characteristic length of the material.

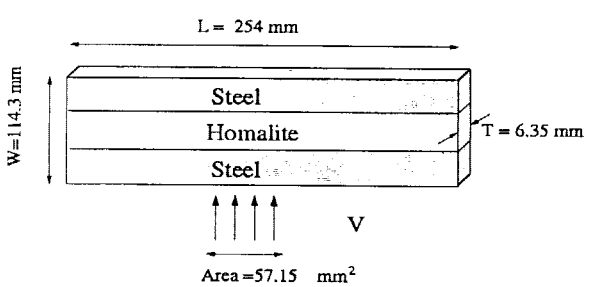

Fig. 1 Geometry for a typical specimen (three layers with equal thickness) used in the experiments of Xu and Rosakis

Table 1. Elastic material properties for Homalite-100 and 4340 Steel

Material		Homalite-100	4340 Steel
Young's modulus	$E\ (GPa)$	5.3	208
Poisson's ratio	ν	0.35	0.3
Mass density	$\rho\,(kg/m^3)$	1230	7830
Longitudinal speed	$c_d\,(m/s)$	2200	5500
Shear wave speed	$c_s\,(m/s)$	1255	3320
Rayleigh wave speed	$c_R\,(m/s)$	1185	2950

Table 2. Fracture and cohesive parameters for Homalite-100, 4340 Steel and Weldon-10

Material		Homalite-100	4340 Steel	Weldon-10
Tensile strength	σ_c (MPa)	35	1490	14
Shear strength	τ_c (MPa)	40	1054.0	22
Fracture energy	G_c (N/m)	88.1	10620	45.0
Opening displacement	δ_c (μm)	6.6	14.3	176.6
Characteristic length	R (mm)	2.8	14	18

Experimental technique

Photo-elasticity is an experimental technique for stress and strain analysis that is particularly useful for members having complicated geometry, complicated loading conditions, or both. The photo-elastic method is based upon a unique property of some transparent materials, in particular, some plastics. When the model is stressed and a ray of light enters along one of the directions of principal stress, the light is divided into two component waves, each with its plane of vibration (plane of polarization) parallel to one of the remaining two principal planes (on which shear stress is zero). Furthermore, the light travels along these two paths with different velocities, which depend on the magnitudes of the remaining two principal stresses in the material, so the waves emerge with relative retardation, which is the number of wave cycles experienced by the two rays traveling inside the body. The two waves are brought together in the photo-elastic polari-scope, and permitted to come into optical interference. A photo-elastic pattern, iso-chromatic pattern of dark and light bands called *fringes* is formed, and it is related to the stress system by the stress-optic law in plane stress configuration [1].

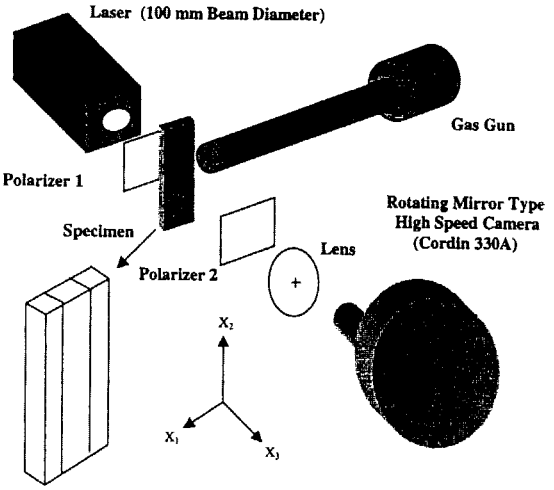

Fig. 2 Schematic of the dynamic photo elasticity setup (Xu and Rosakis)

A schematic setup of the photo-elasticity technique is given in Fig. 2. Two sheets of a circular polarizer were placed on both sides of the specimen. An Innova Sabre argon-ion pulsed laser

served as the light source. The coherent, monochromatic, plane-polarized light output was collimated to a beam of 100 mm diameter. The laser beam was transmitted through the specimen, and the fringe patterns were recorded by the high-speed camera. During the impact test, the projectile was fired by a gas gun and hit the specimen on the side to trigger the recording system. Under dynamic deformation, the generation of iso-chromatic fringe patterns is governed by the stress optic law. For the case of monochromatic light, the condition for the formation of fringes can be expressed as

$$\sigma_1 - \sigma_2 = \frac{Nf_\sigma}{h} \tag{1}$$

where $\sigma_1 - \sigma_2$ is the principle stress difference of the stress tensor averaged through the thickness; f_σ is the material fringe constant associated with the incident light wave length ($f_\sigma = 23.7kN/m$ for Homalite-100); h is the thickness of the specimen; N is the number of fringes. The iso-chromatic fringe patterns observed are proportional to the contour levels of the maximum shear stress, i.e., $\tau = (\sigma_1 - \sigma_2)/2$.

FINITE ELEMENT MODEL

The experiments of Xu and Rosakis were simulated by recourse to a finite element discretization of the continuum. In order to simulate crack initiation and growth, the cohesive model proposed by Camacho and Ortiz [5], and subsequently extended to three dimensions by Ortiz and Pandolfi [6], were emloyed. In adopting a cohesive description of fracture, the formation of a crack is regarded as a gradual process of separation, either by opening or by shearing, leading to the formation of new free surfaces. The cohesive law furnishes the traction vector $\underline{t}$ across the cohesive surface as a function of the opening displacement $\underline{\delta} = [\![\underline{u}]\!]$. Following Camacho and Ortiz [5], this cohesive behavior is formulated in terms of the effective opening displacement

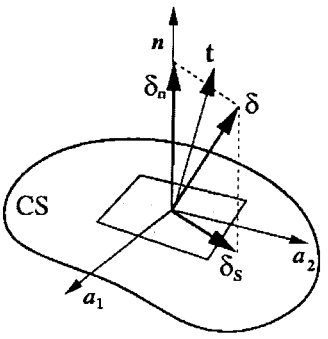

Fig. 3 Decomposition of the opening displacement.

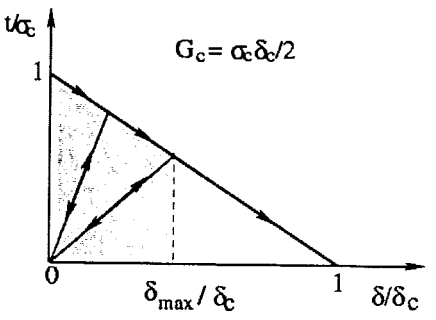

Fig. 4 Linearly decreasing cohesive law.

$$\delta = \sqrt{\beta^2 \delta_S^2 + \delta_n^2} \tag{2}$$

$\delta_n = \underline{\delta} \cdot \underline{n}$ is the normal component of the opening displacement and $\delta_S = |\underline{\delta} - \delta_n \underline{n}|$ is the shear component magnitude of the tangential opening displacement, see Fig.3. The cohesive behavior under monotonic loading is then assumed to be governed by a cohesive potential. The resulting tractions are of the form:

$$\underset{\sim}{t} = \frac{\partial \phi}{\partial \underset{\sim}{\delta}} = \frac{t}{\delta}(\beta^2 \underset{\sim}{\delta_S} + \delta_n \underset{\sim}{n}) \tag{3}$$

where $t = \sqrt{\beta^2 t_S^2 + t_n^2}$ is an effective cohesive traction. Here $t_n = \underset{\sim}{t} \cdot \underset{\sim}{n}$ is the normal component of the cohesive traction and $t_S = |\underset{\sim}{t} - t_n \underset{\sim}{n}|$ is the magnitude of the tangential opening traction. It follows from Eqn. 3 that the parameter β measures the ratio of shear and normal cohesive strength of the material. It also roughly defines the ratio of K_{IIc} to K_{Ic} of the material [2]. The particular monotonic envelope adopted in calculations is shown in Fig. 4. Thus, potential cohesive surfaces are assumed to be rigid up to the attainment of the cohesive strength σ_c, and the effective cohesive traction to subsequently decrease linearly and vanish upon the attainment of a critical effective opening displacement δ_c. The resulting fracture energy of the material is $G_c = \sigma_c \delta_c / 2$, [6]. The cohesive element is rendered irreversible by unloading to the origin from the monotonic envelop just described, Fig. 4. It bears emphasis that upon closure, the cohesive surfaces are subjected to the contact unilateral constraint, including friction. Contact and friction are regarded as independent phenomena to be modeled outside the cohesive law.

NUMERICAL RESULTS

Mesh description

In order to reduce the computational effort, without losing correspondence with the experimental counterparts, a slice of the specimen, 1.6 mm thick (1/4 of the real specimen thickness), is modelled. The out of plane displacements along the surfaces of the plate are constrained to avoid buckling. The computational mesh comprises 65365 nodes and 32482 10-node quadratic tetrahedrons, Fig. 5. The core is modeled using a uniform minimum mesh size of 0.8 mm; the mesh coarsens in the steel layer, with one tetrahedral element across the thickness. The cohesive elements are adaptively inserted along previously coherent interfaces when the local effective stress attains a critical value [6].

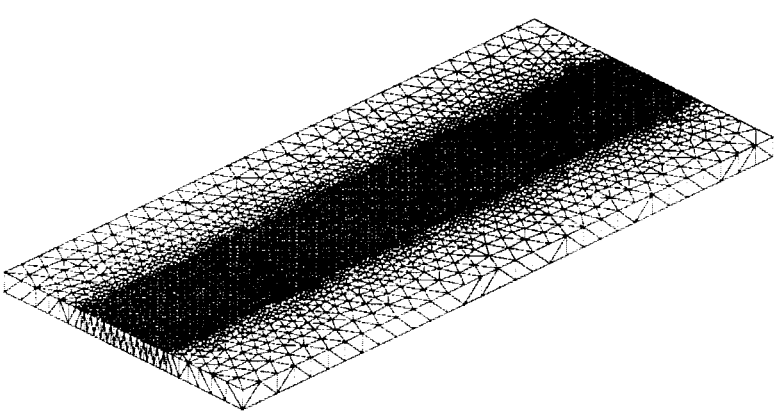

Fig. 5 Computational mesh comprising 65365 nodes and 32482 tetrahedrons.

Boundary and loading conditions

The effect of the bullet impact is approximated by prescribing a velocity profile to the nodes lying on the contact area. The load history is presented in Fig. 6. The impulse duration t_p is 18.4 μs, estimated from the bullet length; both the rise time t_r and the step down time t_d are 2 μs. The impact speed assumed in the calculation is 32.4 m/s. The analysis has been conducted up to 300 μs after impact, with a stable time step of 0.01 μs.

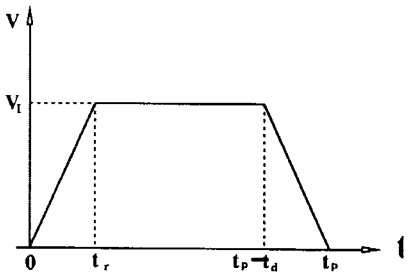

Fig. 6 Impact velocity profile, with rising time t_r = 2 μs, stepping down time t_d = 2 μs; the impulse time t_p =18.3 μs.

Typical failure patterns

The typical failure sequence observed in the experiments of Xu and Rosakis [1] is sketched in Fig. 7. One of the major conclusions of Xu and Rosakis is that shear-dominated inter-layer (or interfacial) cracks are the ones that initiate first and that such cracks grow very dynamically, their speeds and shear nature being enhanced by the large wave mismatch between the core and the face-sheets (the ratio of shear wave speeds of steel to Homalite is 2.6, Table 2). It is the kinking of these cracks into the sandwich core that triggers the complex mechanisms of intra-layer failure.

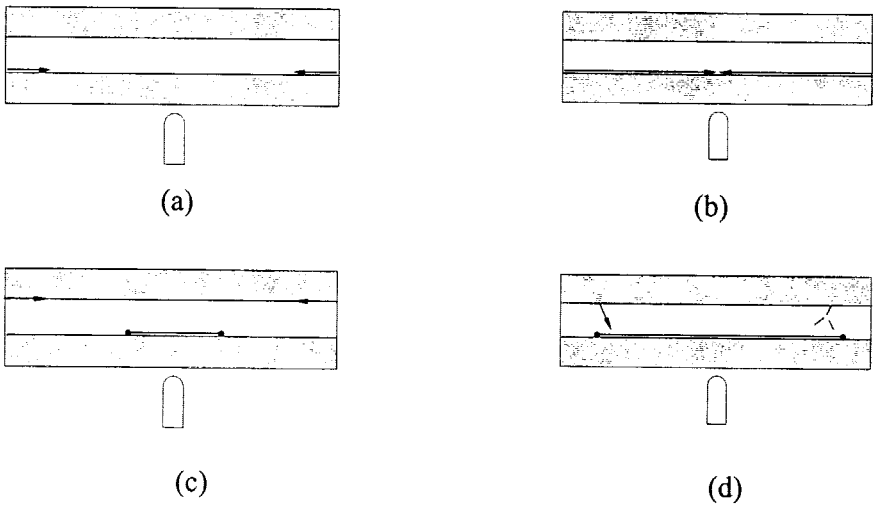

Fig. 7 Typical failure sequence observed in the experiments of Xu and Rosakis, where the arrows indicate the direction of the crack propagation, while the central line in (c) and (d) depicts the Rayleigh wave propagation after the interface separation.

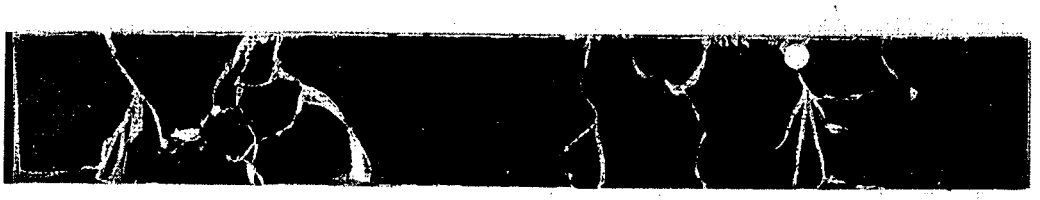

Fig. 8 Typical crack patterns of the core material Homalite-100, observed in the experiments.

At the end of the experiments, the specimens were completely broken, the pieces were collected and glued together to give a crack pattern, and one of those specimens is depicted in Fig.8. The damage sequence was caught by the rotating mirror shown in Fig. 2. It is observed that the damage patterns are not necessarily symmetric because of small variations of loading conditions.

In order to facilitate the view of numerical crack patterns, the highlighted contour plots of a damage variable, which is defined as the ratio between the consumed cohesive energy and the total fracture energy per unit surface (critical energy release rate G_c), were applied. The comparison between the experimental and numerical crack patterns in the same observation window is shown in Fig. 9.

Through the photo-elastic facility, the early stages of the damage pattern were recorded. Fig. 9 shows the experimental fringe pattern and the numerical contour plots of maximum shear stress at about 42 μs after impact. Note the clear shock wave pattern in both cases. This implies that the crack propagates at a velocity above the shear wave speed of the core material Homalite, and is therefore inter-sonic.

(a) (b) (c)

Fig.9 (a) Observation window; (b) experimental fringe patterns; (c) numerical contour plots of maximum shear stress at 42 μs after impact.

Dynamic crack arrest and re-initiation

In order to have a closer look of the crack speed history, the crack initiated from the left edge of the lower interface was chosen to compare with the experimental results in Fig. 10. One can

notice that the crack speed along the lower interface reaches the Rayleigh wave speed soon

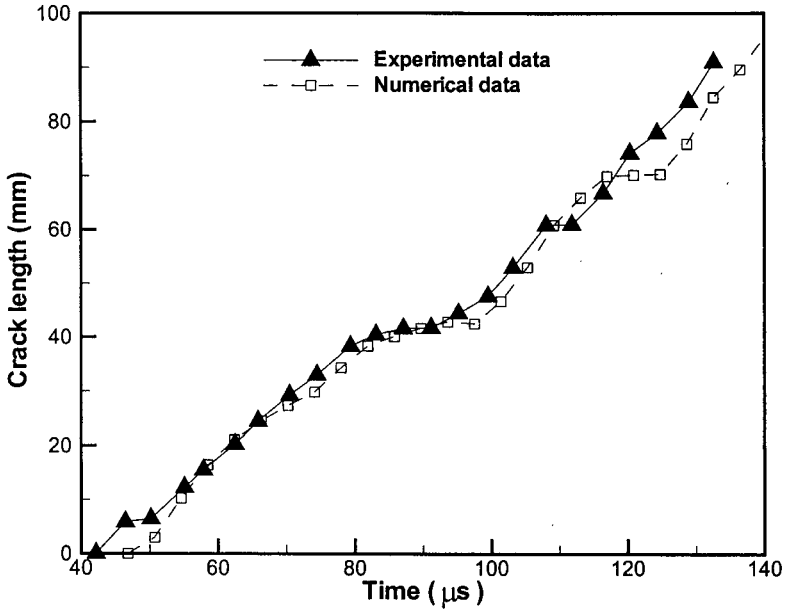

(a)

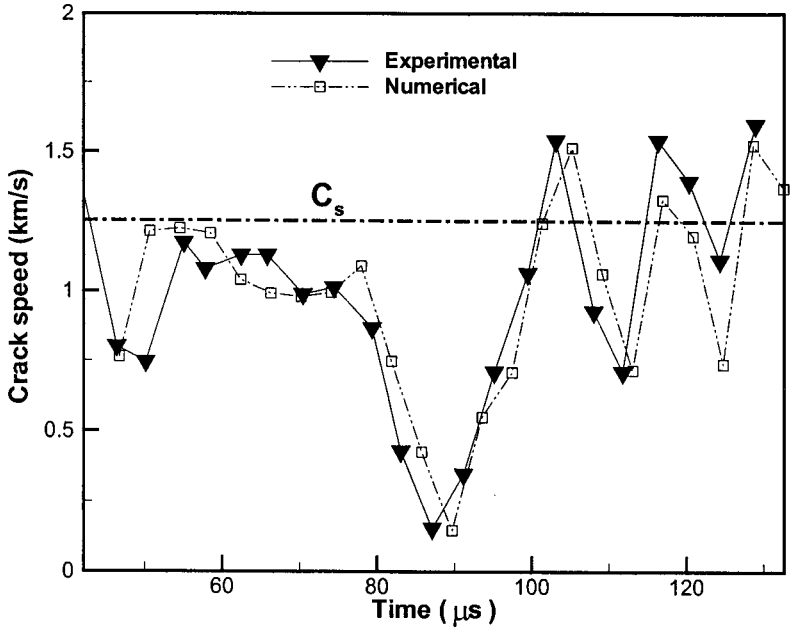

(b)

Fig. 10 Crack-tip position (a) and crack speed (b) history of the lower interface, comparison between experimental (filled triangles) and numerical (empty squares) results.

initiation and drops to a very low value around 90 μs after impact (the plateau part in Fig. 10, both numerical and experimental); next, it increases again dramatically up to the shear wave speed of Homalite-100. In previous research on interfacial cracks, Lambros and Rosakis [8] showed that as soon as an interfacial crack accelerates to the Rayleigh wave speed, it keeps a stable speed as long as constant energy is provided to the crack tip. If the energy supply is suddenly increased, the crack accelerates unstably to another discreet constant level within the inter-sonic regime, otherwise if an unloading wave reaches the crack tip, the crack quickly arrests. Here the complex wave interaction and structural vibration response would result in temporary loss of driving force which accounts for the observed crack arrest and re-initiation.

The effects of the interfacial strength and impact speeds

The effects of different interfacial strengths and impact speeds were also investigated. The results show that even small variations in impact speed and bond strength could substantially influence the initiation behavior of de-lamination (location and nucleation time) and lead to substantially different inter-layer crack speed histories and therefore influence the timing sequence and final extent of subsequent intra-layer damage within the sandwich structures, Fig. 11-12, which agrees very well with the observations by Xu and Rosakis [1].

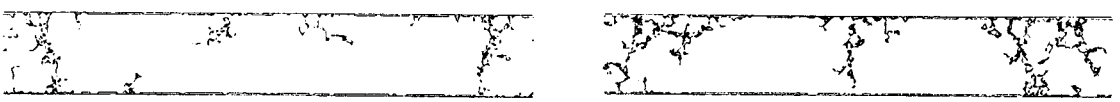

(a) (b)

Fig.11 Numerical crack patterns at time 300 μs after impact, with the same shear strength τ = 22 MPa, for impact speed of (a) 33 m/s and (b) 46 m/s.

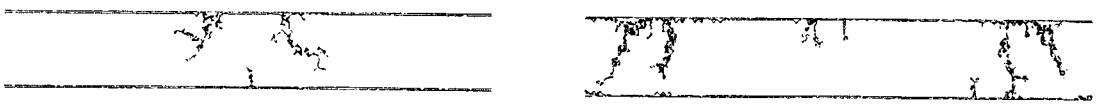

(a) (b)

Fig. 12 Numerical crack patterns at time 300 μs after impact, with impact speed 33 m/s, for inter-facial shear strength of (a) τ = 22 MPa and (b) τ = 7.74 MPa.

SUMMARY AND CONCLUSIONS

The model experiments of Xu and Rosakis on low-speed impact over sandwich structures were simulated applying cohesive models. The simulation captures qualitatively the main experimental observations. The most relevant correspondence is in the development of the first crack at the interface between the layers, the presence of shear stresses along the interface, which renders the crack shear driven and often inter-sonic, and the transition between interlayer crack growth and intra-layer crack branching. The effects of impact speed and bond shear strength are also investigated and highly satisfactory predictions are obtained.

ACKNOWLEDGEMENTS

CY thanks *Ministerio de Educacion, Cultura y Deporte*, Spain, for the fellowship SB2000-0191, which makes possible her stay at *ETSI de Caminos, C., y P., Universidad de Castilla-La Mancha* (UCLM). She also acknowledges the financial support from the *Vicerrectorado de Investigacion* of UCLM. CY and MO are grateful for DOE support provided through Caltech's ASCI/ASAP Center for the Simulation of the Dynamic Response of Solids. AJR acknowledge the support of the Office of Naval Research through grant N00014-9 to Caltech and the support of the National Science Foundation grant CMS9813100.

REFERENCES

1. Xu, L.R. and Rosakis, A.J. (2002), *Int. J. Solids Structures,* 39 (16).
2. Ruiz, G., Pandolfi, A. and Ortiz, M. (2000) *Int. J. Numer. Methods Engrg.* 48(7).
3. Yu, C., Pandolfi, A., Ortiz, M, Coker, D. and Rosakis, A. J. (2002) *Int. J. Solids Structures,* 39(25).
4. Mi, Y., Crisfield, M.A., Davies, Gao and Hellweg, H.B. (1998) *J. Compos. Mater.* 32(14).
5. Camacho, G.T. and Ortiz, M. (1996) *Int. J. Solids Structures,* 33 (20-22).
6. Pandolfi, A. and Ortiz, M. (1998) *Engrg. Comp.* 14 (4).
7. Ortiz, M. and Pandolfi, A. (1999) *Int. J. Numer. Methods Engrg.* 44.
8. Lambros, J. and Rosakis, A.J. (1995) *Proc. Roy. Soc. London* A451.